J. Electrochem. Sci. Eng. **1(1)** (2011) 39-54; doi: **10.5599/jese.2011.0004**

Open Access : : ISSN 1847-9286
www.jESE-online.org

Original scientific paper

External control of anodic dissolution mechanisms of 100Cr6 in nitrate/chloride mixed electrolytes

ANDREAS LESCH, GUNTHER WITTSTOCK✉, CHRIS BURGER*, BENJAMIN WALTHER* and JÜRGEN HACKENBERG*

Department of Pure and Applied Chemistry, CIS - Center of Interface Science, Faculty of Mathematics and Natural Sciences, Carl von Ossietzky University of Oldenburg, D–26111 Oldenburg, Germany
**Robert Bosch GmbH, Stuttgart, Germany*

✉Corresponding Author: gunther.wittstock@uni-oldenburg.de; Tel.: +49 441 7983971; Fax: +49 441 7983979

Received: June 17, 2011; Published: August 20, 2011

Abstract

The anodic dissolution of 100Cr6 steel in neutral electrolytes containing sodium chloride and sodium nitrate was investigated potentiodynamically and galvanodynamically with a rotating disc electrode at room temperature. The total concentration of the mixed electrolyte was 3 mol L^{-1} with variation of chloride/nitrate mole ratios. The potentiodynamic linear sweep voltammograms (LSVs) in mixed electrolytes are similar to the LSVs in pure chloride electrolyte at lower current densities and switch to behaviour observed in pure nitrate electrolytes at higher current densities. Provided that both anions are present, it seems that the dissolution reactions at the steel anode are determined by the interface layer only. The effect of these layers on surface quality and current efficiency was also investigated in a flow channel applying galvanostatic pulses. An evidence for different dissolution mechanisms can be seen with an important influence of duty cycle and flow conditions. This allows external control of the desired dissolution mechanism in mixed electrolytes.

Keywords

Electrochemical machining; Mixed electrolyte; Anodic dissolution; Rotating disc electrode; Flow channel; Galvanostatic pulses

1. Introduction

Electrochemical machining (ECM) is often applied to deburring and shaping components made of e.g. iron and steels in aqueous inorganic salt electrolytes[1,2]. Shape and surface of work pieces are modified by high rate anodic dissolution at high current densities (10-150 A cm^{-2}) with a special

designed cathode as tool. The resulting gap width is usually below one millimetre. High electrolyte flow velocities (5-50 m s^{-1}) are required to remove reaction products and Joule heat. The precision of pulsed ECM is higher compared to direct current ECM because reaction products can be removed during pulse off time [3]. Sodium chloride and sodium nitrate are often used as electrolytes in industrial ECM because of low costs and labour safety aspects. Anodic dissolution of iron and many steels in pure sodium chloride and in pure sodium nitrate electrolytes has been investigated in great detail [4-9]. The dissolution mechanisms in both electrolytes differ strongly and result in very different features of the machined work piece. In chloride media an active anodic dissolution takes place whereas nitrate anions cause a passivation of the substrate surface and transpassive dissolution can be observed. Methods of characterizing the dissolution mechanism are anodic polarization curves, analysis of the resulting surface quality and weight-loss measurements in order to determine the current efficiency. The anodic dissolution of pure iron in chloride electrolyte is divalent over a wide range of current density and the current efficiency is closely to 100 % [5]. Hydrogen is developed in the counter reaction at the cathode [10]. In nitrate media the evolution of oxygen takes place as a second import anodic reaction and the anodic dissolution of iron leads simultaneously to Fe^{2+} ions and Fe^{3+} ions [8,11,12]. At low current densities the iron dissolution efficiency is close to zero because the anodic current originates from oxygen evolution. With increasing current density the current efficiency of the anodic iron dissolution increases up to 90 % but oxygen evolution is still present [11]. The reduction of nitrate anions takes place at the cathode [1].

The anodic dissolution of iron and many steels is mass transport-controlled and reaction products enrich at the anode interface [5,6]. Electrochemically inert metal carbides cause an apparent higher current efficiency for carbide-containing steels because the measured weight-loss includes the mass of carbide particles that were detached but not dissolved during the ECM treatment [13,14]. Qualitative anodic dissolution models explain the observed dissolution behaviour and the resulting surfaces. A two-layer model explains the dissolution in nitrate electrolyte [8,15,16]. Because of the current density-dependent divalent/trivalent dissolution of iron, different iron oxides (Fe_2O_3 and Fe_3O_4) are formed and cover the steel surface as a thin film. An adherent liquid polishing film consisting of supersaturated iron nitrate hydrates is built at the oxide/electrolyte interface and causes a decreasing oxygen evolution rate [11,16]. In chloride media a weakly attached, easily removable black, carbide-rich solid surface film and a thin polishing film consisting of $FeCl_2$, $Fe(OH)_2$ and FeO ($Fe_xO_yCl_z$) are formed at the active-steel-anode/electrolyte interface [14]. In NaCl electrolyte the dissolution rate is higher than in $NaNO_3$ electrolyte due to active dissolution and high current efficiency while in $NaNO_3$ electrolyte a much better dimensional control can be reached.

The anodic dissolution of mild steel in chloride/nitrate mixed electrolytes has been described by Hoare, LaBoda and Mao [17,18]. From their steady-state anodic polarization curves, film stripping and current efficiency measurements, they concluded that chloride anions cause only a localized attack of passive films formed in the presence of nitrate anions on the steel surface. Depending on the chloride/nitrate ratio, the chloride anions lower the oxidation power of the nitrate anions, prevent the formation of a compact, protective film and only a non-protective salt film is present and the resulting surfaces are severe cratered. At lower potentials an active dissolution caused by the chloride anions takes place while passivation and transpassive dissolution dominates the behaviour at more positive potentials. With increasing chloride/nitrate ratio, the work piece surface is passivated at higher potentials [18]. Chloride/nitrate mixed electrolyte have been used

in pulse and pulse reverse through-mask ECM of channels for flow field in stainless steel bipolar plates for PEM fuel cells [19], where the process improved the surface roughness of the channels at the expense of the process time and the rib/channel width uniformity compared to the process in pure chloride electrolyte.

According to the reported results from Mao et al [18] we describe in this paper more detailed insights and process conditions under which the dissolution mechanism of soft annealed steel in chloride/nitrate mixed electrolytes can be externally controlled, i.e. switched between two mechanisms. The influence of varying flow conditions at a rotating disc electrode and in a flow channel as well as the influence of applied potentiodynamic, galvanodynamic and galvanostatic pulse series show clearly the possibility to switch in one and the same electrolyte exclusively by external control (current or voltage, hydrodynamics) between both dissolution mechanisms allowing fast machining rates using the chloride mechanism and high precision by the nitrate mechanism in order to obtain crater-free surfaces.

Experimental

Specimens

Spheroidization-annealed 100Cr6 cylinders (annealed to globular cementite, 5 mm diameter) were used as specimens from which the cross sectional surfaces were investigated. The 100Cr6 steel is mainly composed of approximately 96 wt. % iron, 1.5 wt. % chromium and 1 wt. % carbon. Carbon is contained as C in the steel matrix (20 % of total C content), as globular Fe_3C (40 % of total C content) with diameters of approximately 1-3 µm and as 100 nm-slices $Fe_{2.5}C$ (40 % of total C content). The metal carbides were considered to be electrochemically inert under the applied conditions. Directly before and after the experiments the specimens were washed with distilled water and isopropanol.

Electrolytes

Aqueous solutions of sodium chloride and sodium nitrate served as electrolytes. The total salt concentration c_{tot} was set to 3 mol L^{-1} with variation of chloride/nitrate mole ratio. The chloride/nitrate concentration ratio is given as the relative chloride concentration θ (Eq. 1).

$$\Theta = \frac{c_{Cl^-}}{c_{tot}} \tag{1}$$

The electrolyte temperature was (23±1) °C. With increasing θ the measured conductivity increases from 156 mS cm^{-1} (θ = 0) up to 194 mS cm^{-1} (θ = 1).

Rotating disc electrode (RDE)

The measurements of potentiodynamic and galvanodynamic scans or cyclic voltammograms (CVs) were performed with a rotating disc electrode and potentiostat VoltaLab 80 PGZ402 & VoltaMaster4 Software (Radiometer Analytical SAS). The front surfaces of the 100Cr6 specimens were ground mechanically with SiC papers and the cylinder barrels were masked with an insulating galvanic polyester tape before each measurement. These samples were used as working electrodes (WE) in a three electrode cell completed by a platinized titanium net as counter electrode (CE) and an Ag/AgCl/sat. KCl reference electrode (RE). WE and CE had an electrode distance of approximately 1 cm. The scan rate for potentiodynamic experiments was set to 50 mV s^{-1}. In this paper all potentials *E* are referred to the standard hydrogen electrode (SHE). Under the

typical rotation rate of 3000 rpm laminar flow conditions are expected. Incipient turbulences must, however, be expected because of grinding marks at the work piece surface, roughness due to anodic dissolution and recess of the surface below the galvanic polyester tape used to mask the side walls of the sample cylinders.

Flow channel

A flow channel in form of a parallel plate reactor was used. The flow velocity was set to 7 m s^{-1} assuming turbulent flow conditions [20]. Mechanical grinding was done for preparation of the specimens. A steel cathode with 5 mm diameter was positioned directly opposite to the 100Cr6 specimen with a gap of 0.75 mm before start of anodic dissolution. The electrodes were fixed and, therefore, the gap width increased during experiments. With this two-electrode configuration galvanostatic pulses up to 40 A cm^{-2} were applied with a custom made galvanostat (plating electronic GmbH, Germany). No current was applied during pulse off time. The pulse times were in the range of milliseconds. The duty cycle γ is

$$\gamma = \frac{t_{on}}{t_{on} + t_{off}} \tag{2}$$

t_{on} is the pulse on time and t_{off} is the pulse off time. An averaged current i_d can be calculated with γ and pulse current i_p (Eq. 3 [21]).

$$i_d = i_p \cdot \frac{t_{on}}{t_{on} + t_{off}} = i_p \cdot \gamma \tag{3}$$

Multiplying i_d with measuring time t_{tot} gives flowing charge Q (Eq. 4):

$$Q = i_d \cdot t_{tot} \tag{4}$$

The theoretical weight loss Δm_{theo} was calculated by the Faraday law (Eq. 5):

$$\Delta m_{theo} = \frac{i_d \cdot t_{tot} \cdot M}{z \cdot F} = \frac{Q \cdot M}{z \cdot F} \tag{5}$$

where M is the molar mass of iron and F is the Faraday constant. The dissolution valence z was taken as 2 in all calculations knowing that the valence is between 2 and 3 in $NaNO_3$ electrolyte depending on current density [11]. Current efficiency η is then given by equation 6:

$$\eta = \frac{\Delta m_{tot}}{\Delta m_{theo}} \cdot 100\%. \tag{6}$$

where Δm_{tot} is the total experimental mass loss of the specimens which was obtained as mass difference before and after the dissolution. Duty cylces γ of 0.625, 0.5 and 0.167 were applied with charges Q between 50 and 300 C.

Surface characterisation

Observation with optical microscopes was used for rough classification of the dissolution mechanisms. The topography of the surface was measured with confocal microscope nanofocus µsurf (NanoFocus AG), for which regions in the middle of the surface were chosen at which minor streaming artefacts occur. The 3D average roughness S_a was then calculated with software nanoExplorer XT. The topography was filtered in waviness and roughness by a robust Gauss-filter

with a cut-off wavelength of 0.25 mm. S_a is the arithmetic mean of the absolute distances of the surface points from the mean plane and is given by equation 7:

$$S_a = \frac{1}{NL}\sum_{j}^{N}\sum_{i}^{L}|Z|\left(x_j, y_i\right) \quad (7)$$

N and *L* are the indexes of measured points in *x*- and *y*-direction. This method facilitates a relative comparison of the resulting surface roughnesses. Additionally, the resulting surfaces were examined with scanning electron microscope (SEM) EVO 50 VPX (Carl Zeiss AG). An Everhart-Thornley-detector and an acceleration voltage of 20 kV were used for 1000× enlargement with a work distance of 10 mm.

Results and Discussion

Sharp transition from active to transpassive dissolution at resting electrode

Linear sweep voltammograms (LSV) were recorded between -0.5 V and 7.2 V. Figure 1 shows the LSVs in pure NaCl electrolyte (θ = 1), in pure $NaNO_3$ electrolyte (θ = 0) and in mixed electrolytes with θ = 0.67, 0.5 and 0.33 at a resting electrode.

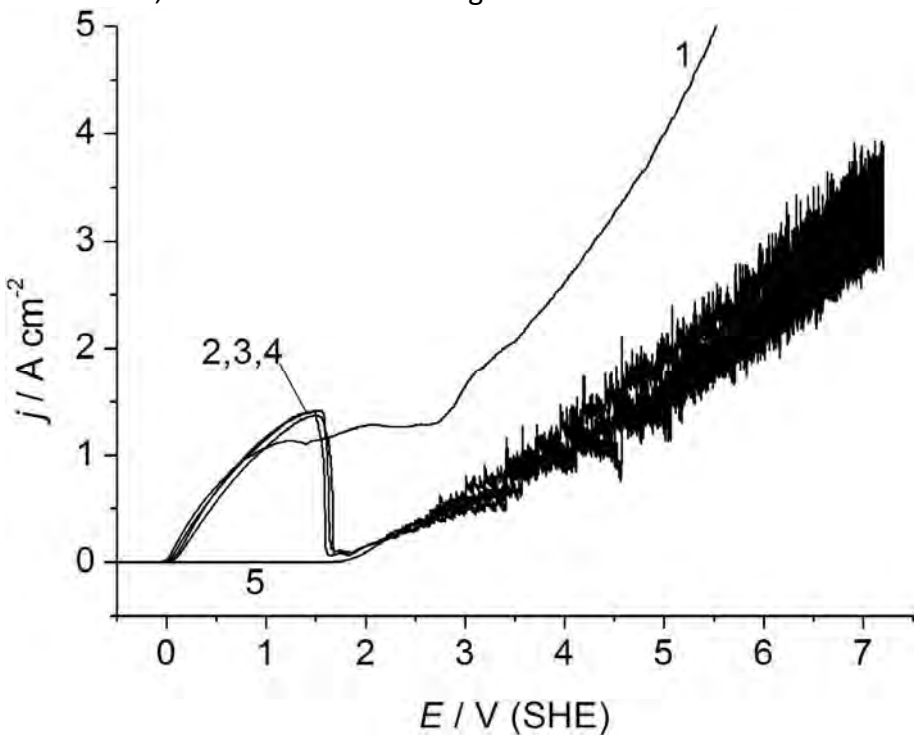

Figure 1. *LSVs in 3 M NaCl, 3 M $NaNO_3$ and in three chloride/nitrate mixed electrolytes; static WE; Scan rate 50 mV s^{-1}; relative chloride concentrations θ: 1 (1), 0.67 (2), 0.5 (3), 0.33 (4), 0 (5).*

The curves of the pure electrolytes show the well known behaviour of active (NaCl) and transpassive dissolution ($NaNO_3$) [1]. In NaCl electrolyte a limiting current is reached because the concentration of reaction products increases to saturation. Thus a limiting current plateau is built until the overlimiting current is reached and the current increases again. In $NaNO_3$ electrolyte fluctuating current densities are caused by the evolution of oxygen at the WE which sets in at 1.8 V. The curves that were measured in the three mixed electrolytes overlap with each other. They agree qualitatively with earlier reports about anodic dissolution in mixed electrolytes [18]. Surprisingly, there is no strong influence of the relative chloride ion concentration on the anodic dissolution at the resting WE in Figure 1. At low potentials active dissolution takes place, indicated

by an increasing current density from 0 V on. The surface is suddenly passivated at approximately 1.6 V and the current density decreases to nearly 0 A cm^{-2}, oxygen evolution starts at 1.8 V and transpassive dissolution sets in at higher current densities. With respect to the models of metal/electrolyte interface [11,14,16] the following mechanistic model can be proposed. At lower current densities which occur at potentials below 1.6 V at the resting electrode, the dissolution mechanism must be dominated by the chloride anions and the LSV is very similar to the curve in pure chloride solution. In this paper this section of LSVs will be called "chloride curve". Due to active dissolution, the chloride polishing film is formed. The nitrate anions are larger than chloride anions. Most likely their incorporation in the polishing film changes the structure of the polishing film so that no diffusion controlled current regime (plateau in the pure NaCl electrolyte) is observed in mixed electrolytes. The higher the current density, the higher is the active dissolution rate of the steel. Chloride anions have to diffuse from the bulk of the electrolyte through the diffusion layer to the steel surface. When the current density becomes higher than approximately 1.4 A cm^{-2} not enough chloride anions reach the steel surface. Therefore, the nitrate polishing film composed of iron nitrate hydrates is formed. This film could withdraw the water from the chloride polishing layer. Hence, iron chloride could be precipitated and could be displaced by the nitrate polishing film and the anodic dissolution is dominated by the nitrate anions at potentials higher than 1.8 V. Hence, the transpassive dissolution sets in at higher current densities at E > 1.8 V and this section of LSVs is called "nitrate curve" below. The transition from active to transpassive dissolution can also be observed visually (see Figure SM-11 in Supporting Information). During active dissolution the assumed reaction products creep down as a green viscose film. After passivation, the evolution of oxygen breaks off the visible flakes of the black carbide-containing layer from the anode surface. It is suggested that this surface layer is equal to the one in pure NaCl electrolyte. Haisch et al. [7] investigated the surface layer obtained in pure NaCl electrolyte by energy dispersive X-ray microanalysis. They reported that the particles of this layer mainly consist of Fe, Cr and C and suggested that they originate from the carbides in the steel matrix [7]. Transpassive dissolution can be observed by the formation of oxygen bubbles and yellow-brown colouration of the solution.

Influence of anion transport on the transition from active to transpassive dissolution at RDE

For further experiments the WE was operated as RDE in order to improve the removal of oxidation products and simulate the electrolyte flow under technical ECM conditions. This leads to an increasing of limiting current in NaCl electrolyte [22] and to a less fluctuating current density in $NaNO_3$ electrolyte in corresponding LSVs at 3000 rpm (Figure 2).

In pure 3 M NaCl electrolyte no limiting current plateau is observed within the resulting current density range (curve 1). The electrolyte changes its colour from colourless to green and green precipitation occurs. In pure $NaNO_3$ electrolyte the current density rises linearly at 1.8 V (curve 14). Because transpassive dissolution sets in at even higher current densities, the colourless electrolyte changes to yellow-brown and yellow-brown precipitations are observed. With decreasing θ, the activation potential for the chloride dominating activation potential is shifted to more anodic potentials. The nitrate anions disturb the activation [23]. With respect to the proposed mechanistic model, increasing θ leads to higher current densities at which the change of dominating mechanism occurs due to the transport of chloride anions from the bulk of the electrolyte through the diffusion layer to the steel surface. With increasing θ formation of the chloride polishing film can be maintained to higher current densities until replacement by

the nitrate polishing film and commencement of transpassive dissolution. In this paper the term passivation is not used for this phenomenon because the current density does not fall to nearly zero for $\theta \geq 0.07$. Transpassive dissolution sets in directly. The LSVs in mixed electrolytes with $\theta > 0.83$ indicate no sharp decrease in current density. Both mechanisms compete and the relatively small concentration of nitrate anions cannot create an abrupt change of the dominating mechanism. Curve 13 shows that for $\theta = 0.03$ the flux of chloride ions is too small to induce and maintain active anodic dissolution in comparison with $\theta = 0.05$ (curve 12). The insert in Figure 2 shows separate forward and backward LSV in mixed electrolyte with $\theta = 0.5$ arranged like a CV. The backward LSV corresponds completely to the backward LSVs which are obtained in pure $NaNO_3$ electrolyte due to stable transpassive dissolution.

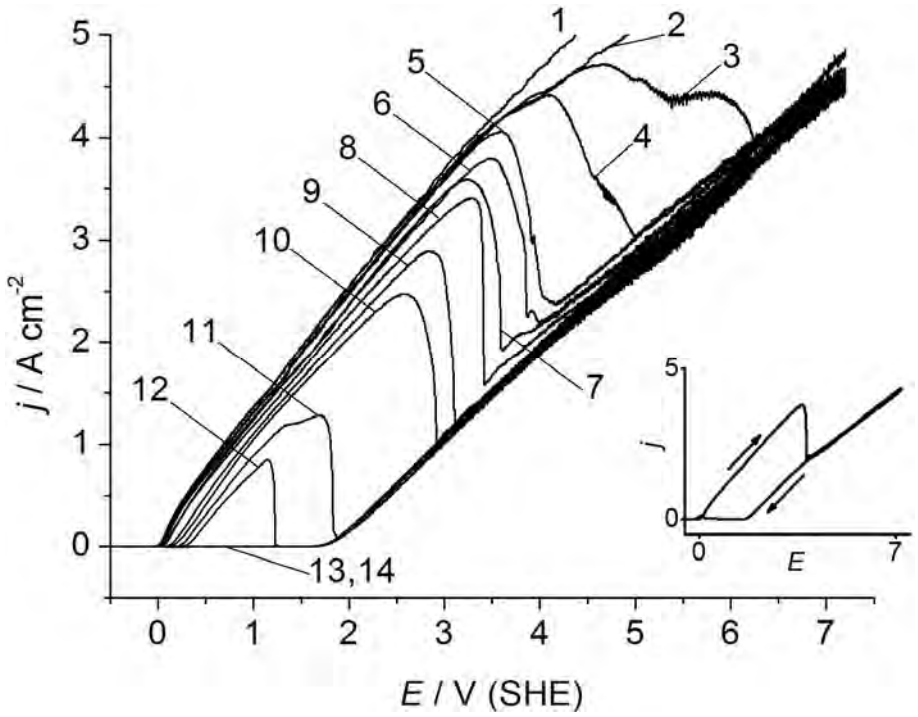

Figure 2. *LSVs; rotation rate of WE 3000 rpm; scan rate 50 mV s^{-1}; relative chloride concentrations* θ*: 1 (1); 0.9 (2); 0.87 (3); 0.83 (4); 0.77 (5); 0.67 (6); 0.5 (7); 0.33 (8); 0.13 (9); 0.1 (10); 0.07 (11); 0.05 (12); 0.03 (13); 0 (14). Insert: forward and backward LSV in mixed electrolyte with* θ *= 0.5.*

The transport of chloride anions and, therefore, the transition from chloride curve to nitrate curve can also be controlled by rotation rate. Increasing the rotation rate for a given $\theta = 0.5$ increases the current density at which the dissolution mechanism changes (Figure 3) due to a higher flux of chloride ions to the surface.

This is in agreement with the proposed mechanistic model. The mass flux of chloride anions J_{Cl^-} to the disc surface can be estimated by using equation 8 [24]:

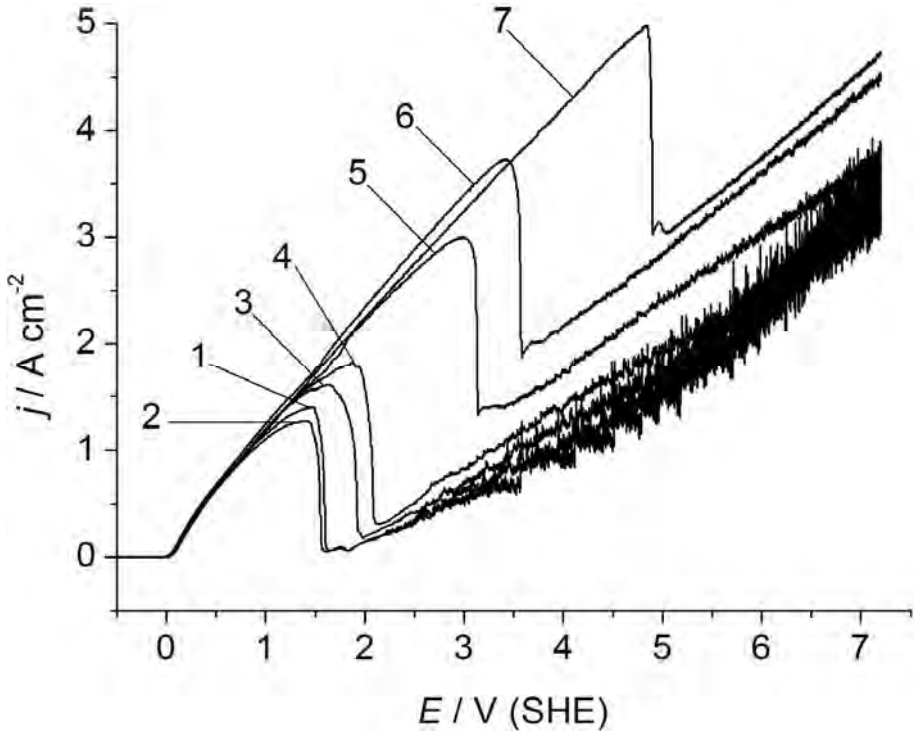

Figure 3. *LSVs in chloride/nitrate mixed electrolyte; θ = 0.5; scan rate 50 mV s^{-1}; rotation rates: 0 rpm (1); 100 rpm (2); 500 rpm (3); 1000 rpm (4); 2000 rpm (5); 3000 rpm (6), 4000 rpm (7).*

$$J_{Cl^-} = 0.62 \cdot D_{Cl^-}{}^{2/3} \cdot \nu^{-1/6} \cdot \omega^{1/2} \cdot c_{Cl^-} \quad (8)$$

where D_{Cl^-} = 2.032·10^{-5} cm^2 s^{-1} [25] is the diffusion coefficient of Cl^- anions at infinite dilution in water. The cinematic viscosity ν = 1·10^{-2} cm^2 s^{-1} [24] is assumed to be the one of water. ω is the angular velocity of the RDE and c_{Cl^-} the bulk concentration of chloride anions. With equation 8 only the diffusion is considered whereas migration is neglected. In the mixed electrolyte with θ = 0.5 the concentration of chloride is 1.5 mol L^{-1}. With rotation rate 3000 rpm and ω = 2·π·3000 rpm = 314.2 s^{-1}, J_{Cl^-} is 2.64·10^{-5} mol cm^{-2} s^{-1} calculated from equation 8. This calculation does not consider the larger existing nitrate anions in the solution. The nitrate anions could act as obstacles for the chloride anions flux but migration could lead to an increase of J_{Cl^-}. Therefore, the calculated mass flux of chloride anions is only an approximation. The dissolution rate of iron J_{Fe2+} at the surface can be calculated by using equation 9, which is derived from Faraday law (Eq. 5):

$$J_{Fe^{2+}} = \frac{j_{Cl^-,lim}}{F \cdot z} \quad (9)$$

where $j_{Cl^-,lim}$ = 3.6 A cm^{-2} is the current density at which the active dissolution mechanism cannot be maintained any longer. The calculated value J_{Fe2+} = 1.87·10^{-5} mol cm^{-2} s^{-1} is in agreement with the proposed model considering that a Fe^{2+} flux of 1.87·10^{-5} mol cm^{-2} s^{-1} would require a Cl^- flux of 2·1.87·10^{-5} mol cm^{-2} s^{-1} to form stoichiometrically $FeCl_2$.

The active dissolution in mixed electrolytes is mass transport-controlled with respect to chloride ions. From the LSV experiments it is concluded that under RDE conditions a sharp distinction is possible between active (chloride anion-dominated mechanism) and transpassive (nitrate anion-dominated mechanism) anodic dissolution mechanisms.

Switching between both mechanisms by potential control at RDE

Sequential LSVs which means in this paper that several LSVs are applied directly one after the other show that switching between the two dominating dissolution mechanisms is easily possible by potential control. The start potential can be chosen in the area of the chloride or the nitrate curve.

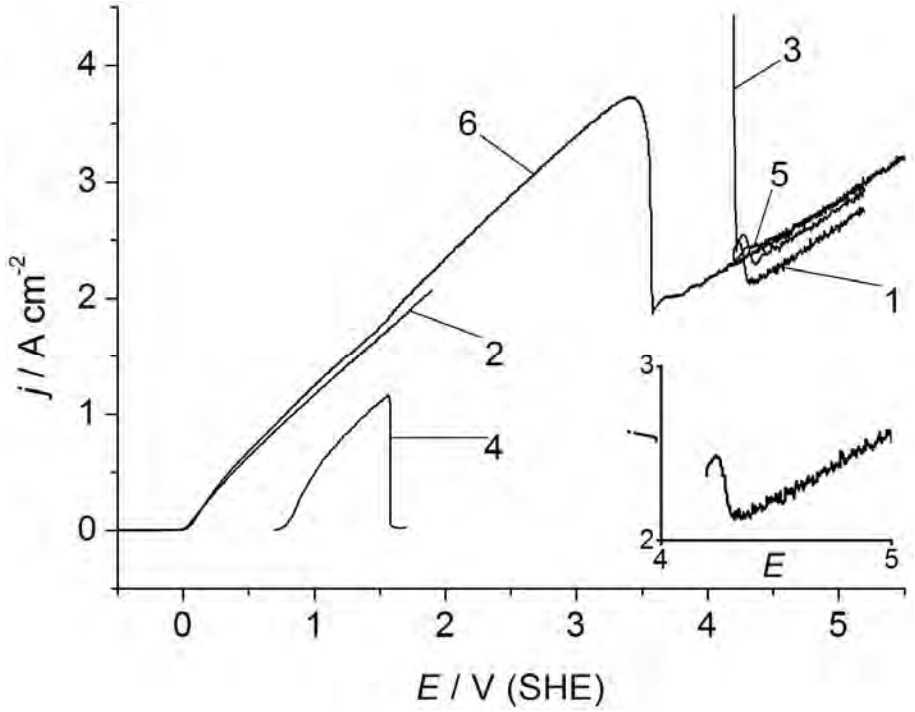

Figure 4. *In sequence (1) to (5) directly successive measured LSVs with potential limits 4.2 V to 5.2 V (1); -0.5 V to 1.9 V (2); 4.2 V to 5.2 V (3); 0.7 V to 1.7 V (4); 4.2 V to 5.2 V (5); complete LSV (6);* $\theta = 0.5$*; rotation rate 3000 rpm; scan rate 50 mV* s^{-1}*. Insert: sequence (1) enlarged.*

Curve 1 of Figure 4 starts in the potential region of the nitrate curve. After a short initial rise of the current density *j* (Figure 4 insert), *j* decreases and the curve follows the nitrate curve. The initial rise of *j* after switching from active to transpassive dissolution is reproducibly observed (curves 3, 6 in Figure 4). The reason of this effect is still unknown. Maybe chloride anions and nitrate anions which are initially present at the anode cause a situation where both mechanisms take place simultaneously. After the chloride anions are consumed, the dissolution follows the nitrate curve. Curve 2, initiated at 0 V, was applied directly after curve 1 and follows exactly the chloride curve. The surface is activated. Stepping the potential to 4.2 V, i.e. to a section of the LSV dominated by the transpassive dissolution, causes a change of dominating mechanism indicated by the large decrease of current density within a very short transition time (curve 3). The resulting current density after that switch is so high that the consumption of chloride ions cannot be maintained by mass transport and active dissolution ceases. Curve 4 starts within the section of the chloride curve (at 0.7 V). An instantaneous slope can be seen before the current density increases linearly with increasing potential. This slope fits to the chloride curve in the complete LSV but the current density is approximately 1 A cm^{-2} lower. It seems that the chloride curve is shifted to more anodic potentials for presently unknown reasons. One explanation could be that an acidification caused by oxygen evolution at anode/electrolyte interface influences the processes and shifts the chloride curve. A passivation is observed at approximately 1.5 V in this curve. So the next linear sweep in section of nitrate curve is following the expected behaviour of transpassive dissolution (curve 5).

Switching between both mechanisms by current density control at RDE

Programmed current chronopotentiometry (PCC) [26], i.e. the linear variation of the current in a galvanodynamic sweep experiment gave similar results like LSVs (see Figure SM-12). At low current densities active dissolution takes place in mixed electrolytes and the potential increases linearly with increasing current density. This section of PCC fits to the PCC in pure NaCl electrolyte. When a certain current density (depending on chloride mass transport) is reached the mechanism switches to transpassive dissolution which is indicated by an abrupt potential increase. From then on, the potential increases linearly with current density like the PCC in pure $NaNO_3$ electrolyte. This is in agreement with the proposed mechanistic model. An example for switching between both dominating mechanisms by current density control is shown in Figure 5.

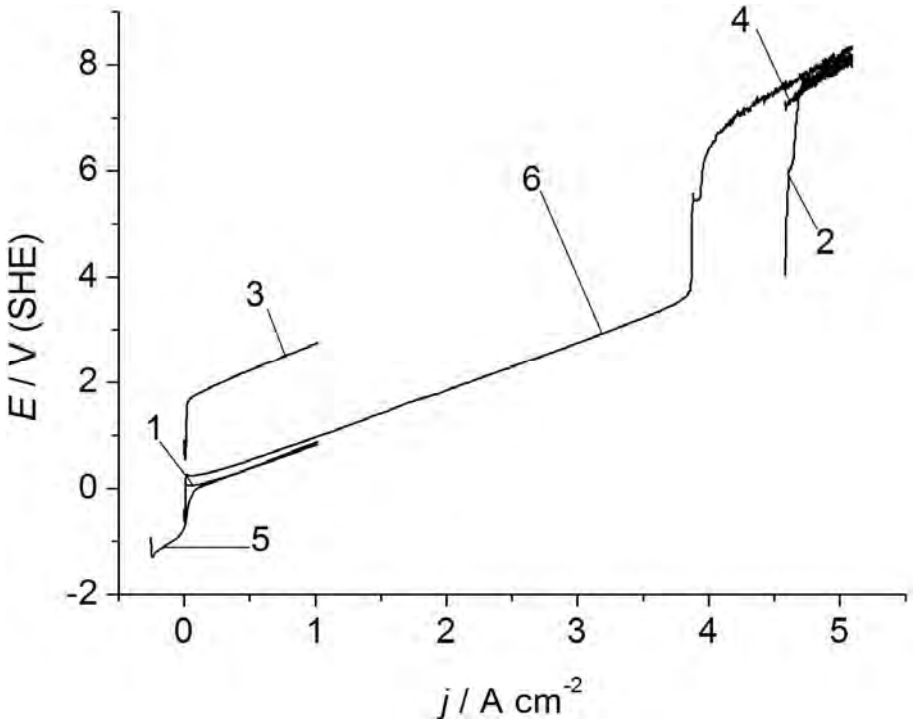

Figure 5. *In sequence (1) to (5) directly successive measured PCCs with current density limits from 0 A cm^{-2} to 1 A cm^{-2} (1); 4.6 A cm^{-2} to 5.1 A cm^{-2} (2); 0 A cm^{-2} to 1 A cm^{-2} (3); 4.6 A cm^{-2} to 5.1 A cm^{-2} (4); 0.3 A cm^{-2} to 1 A cm^{-2} (5); complete PCC (6); θ = 0.5; rotation rate 3000 rpm; scan rate 51 mA cm^{-2} s^{-1}.*

Curve 1 starts at current density of 0 A cm^{-2} and active dissolution sets in immediately. A current density step to 4.6 A cm^{-2} leads to a change of the dominating mechanism to transpassive as expected (curve 2). This is indicated by an abrupt increase of potential. Stepping back to 0 A cm^{-2} (curve 3) leads to a surprising effect. Passivity of the surface does not break down and transpassive dissolution sets in. After a current density ramp in the range of transpassive dissolution (curve 4) a slight cathodic current density of 0.3 A cm^{-2} leads to an activation of the steel surface (curve 5). Curve 6 shows a complete PCC.

From the LSV experiments it is concluded that not only a sharp transition from active to transpassive anodic dissolution due to mass transfer rate of chloride anions occurs, but switching between the dominating mechanisms by potential and current density control is possible as well.

Flow channel experiments

Flow channel experiments permit a more realistic modelling of ECM experiments under various flow conditions using galvanostatic pulses. The anodic dissolution in pure NaCl electroylte, in pure

$NaNO_3$ electrolyte and in mixed chloride/nitrate electrolytes was investigated. It was assumed that flow conditions in flow channel are more turbulent than in RDE experiments. The more turbulent flow causes a thinner diffusion layer and better mass transfer of chloride ions. Therefore, the chloride-dominated mechanism can be maintained at higher current densities, or the chloride-dominated mechanism at a given current density should be sustained by an electrolyte with a lower θ. This hypothesis was tested with relative low values of θ of 0.07, 0.17 and 0.33 by determining the current efficiencies according to equation 6. The dissolution valence *z* was set to 2. Because of other probable reactions, such as the formation of trivalent iron and the formation of trivalent chromium species, the experimental results are useful only for relative comparisons between similar experiments of the same material.

Experiments were performed for pulse current densities *j* of 5, 10, 20 and 40 A cm^{-2} (Figure 6).

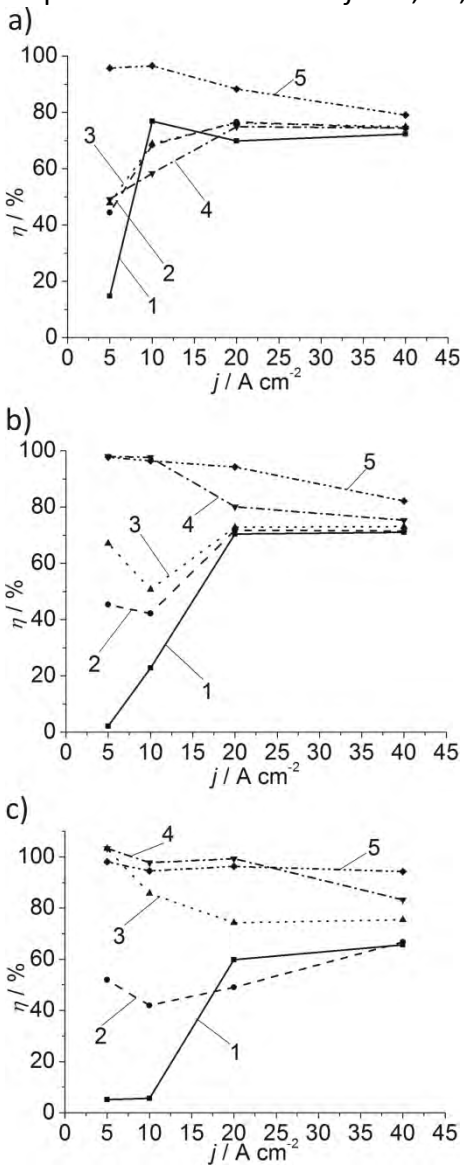

Figure 6. *Current efficiencies* η *with* γ *= 0.625 (**(a)**, 300 C), 0.5 (**(b)**, 100 C) and 0.167 (**(c)**, 100 C); relative chloride concentrations* θ*: 0 (1); 0.07 (2); 0.17 (3); 0.33 (4); 1 (5);* j *= 5 A cm^{-2}, 10 A cm^{-2}, 20 A cm^{-2} and 40 A cm^{-2}; Lines of all styles are guides to the eye.*

The current efficiencies in pure NaCl electrolyte (curves 5) and in pure $NaNO_3$ electrolyte (curves 1) correspond to literature values [11,14,15,20]. In pure NaCl electrolyte η is about 100 %. Decreasing η at higher *j* could be caused by additional formation of trivalent iron. In pure $NaNO_3$ electrolyte it can be distinguished between passivation of the surface, transition zone and

transpassive dissolution. The region of the transition zone is shifted to higher current densities with lower γ. Total experimental mass loss Δm_{tot} includes the erosion of electrochemically inert metal carbides. Often the ratio $\Delta m_{tot}/\Delta m_{theo}$ is quoted as current efficiency that might exceed 100 %. From known carbon content and its compounds Δm_{tot} can be corrected by subtracting the mass of electrochemical inert components Δm_C in order to obtain the carbide-free weight loss Δm by equation 10 (Details in SM-3):

$$\eta_{corr} = \frac{\Delta m_{tot} - \Delta m_{inert}}{\Delta m_{theo}} \cdot 100\% = \frac{\Delta m}{\Delta m_{theo}} \cdot 100\%. \quad (10)$$

For example in pure NaCl electrolyte with γ = 0.625 and 0.167 at 5 A cm^{-2} a $\eta = \Delta m_{tot}/\Delta m_{theo}$ of 112 % and 115 % are measured and yields a corrected η_{corr} of 100 % and 102 %. There is still a trend of η_{corr} being slightly larger than 100 % indicating a more complex dissolution mechanism for 100Cr6.

With γ = 0.625, the current efficiencies in the mixed electrolytes are rather uniform (curves 2 and 4, Figure 6a). At 20 A cm^{-2} and 40 A cm^{-2} η is about 87 % and is approximately the same as in pure $NaNO_3$ electrolyte. This is in agreement with the results of a microscopic inspection of the resulting surfaces at 40 A cm^{-2} with θ = 1, 0.33 and 0 (Figure 7a-c).

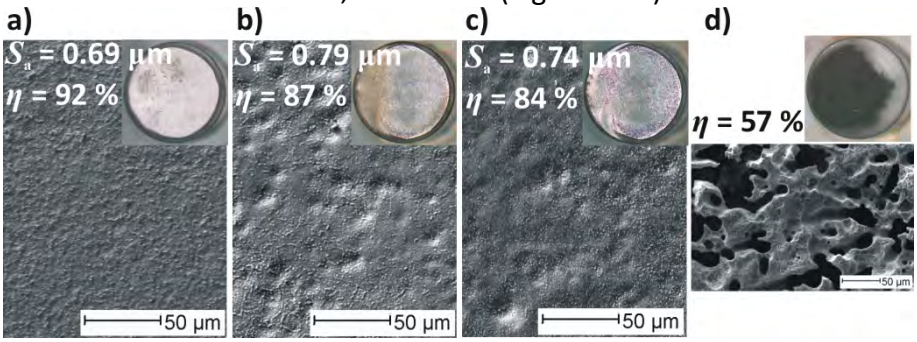

Figure 7. *Optical and SEM micrographs of the resulting surfaces with γ = 0.625. Electrolyte flow direction in optical micrographs and in SEM micrographs is from left to right.* ***(a)*** *j = 40 A cm^{-2}; θ = 1.* ***(b)*** *j = 40 A cm^{-2}; θ = 0.33.* ***(c)*** *j = 40 A cm^{-2}; θ = 0.* ***(b)*** *j = 5 A cm^{-2}; θ = 0.33.*

A very similar appearance of the surfaces is obtained in mixed electrolyte (θ = 0.33, Figure 7b) and in pure $NaNO_3$ electrolyte (Figure 7c). The current efficiencies in the mixed electrolyte and in pure $NaNO_3$ electrolyte (87 % and 84 %, respectively) and the surface roughnesses S_a (0.79 µm and 0.74 µm, respectively) are approximately the same (Figure 7b-c). Moreover, the SEM micrographs appear equal and are distinctly different from those obtained in pure NaCl electrolyte (θ = 1, Figure 7a). These are all indications of a nitrate anion-dominated dissolution mechanism at high current densities which is in line with the RDE results. Embedded small globular carbides can be seen clearly in the SEM micrographs in Figure 7a-c. The influence of additional turbulent flow due to the emerging edge can be seen in the optical micrographs, especially in Figure 7c for θ = 0. The higher material removal at the edge of the samples can be explained by higher current density which can be calculated by secondary current distribution. Applying 5 A cm^{-2} in mixed electrolyte with θ = 0.33 leads to a very porous, black surface structure with deep holes (Figure 7d). The porosity is so high that S_a cannot be measured with confocal microscopy. Instead of a dominating chloride dissolution mechanism it is proposed that both mechanisms proceed simultaneously at different regions of the surface. The current efficiency of 57 % is an indication for that. Active dissolution produces deep holes while the transition zone from passive to transpassive dissolution obtained in pure $NaNO_3$ electrolyte produces the black surface film in between. This black surface

film could correspond to the surface films described by Haisch in direct current experiments in pure $NaNO_3$ [15]. Described simultaneous dissolution by both mechanisms was not seen in RDE experiments. These observations illustrate the importance of flow conditions for the electrochemical dissolution reaction and the turbulence increasing from RDE to flow channel.

With γ = 0.5 the influence of γ becomes apparent. For θ = 0.07 (curve 2, Figure 6b) and 0.17 (curve 3, Figure 6b) there are current efficiencies measured at 5 A cm^{-2} and 10 A cm^{-2} which indicates a simultaneous chloride-dominated and nitrate-dominated dissolution. The current efficiencies at 20 A cm^{-2} and 40 A cm^{-2} approach those in pure $NaNO_3$ electrolyte. With θ = 0.33 (curve 4, Figure 6b) a minor influence of chloride anions is obtained at 20 A cm^{-2} and 40 A cm^{-2} because of little higher current efficiencies than in pure $NaNO_3$ electrolyte (93 % and 88 % compared to 82 % and 83 %). In this mixed electrolyte at 5 A cm^{-2} and 10 A cm^{-2} the anodic dissolution is dominated by chloride anions indicated by current efficiencies, surface roughnesses and the optical impression (Figure 8a-d).

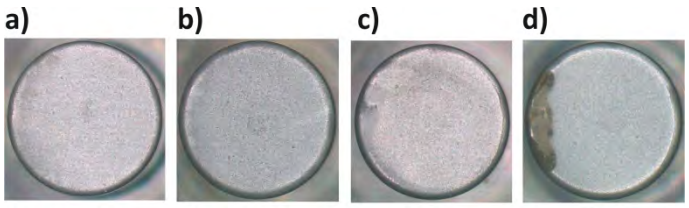

Figure 8. *Comparison of resulting surfaces with* θ *= 0.33 and 1 at 5 A* cm^{-2} *und 10 A* cm^{-2}*;* γ *= 0.5. Electrolyte flow direction in optical micrographs and in SEM micrographs is from left to right.* ***(a)*** j *= 5 A* cm^{-2}*,* θ *= 1.* ***(b)*** j *= 5 A* cm^{-2}*,* θ *= 0.33.* ***(c)*** j *= 10 A* cm^{-2}*,* θ *= 1.* ***(d)*** j *= 10 A* cm^{-2}*,* θ *= 0.33.*

This result is in agreement with the proposed mechanism which is based on the idea of chloride-dominated dissolution mechanism at lower and nitrate-dominated dissolution mechanism at higher *j*. The more pronounced edge effect due to the additional flow effect at the emerging edge can be seen at the surface in mixed electrolyte with θ = 0.33 at 10 A cm^{-2} as well (Figure 8d). Here the surface has a completely different appearance. This is another hint for the importance of flow conditions.

For the duty cycle γ of 0.167 the current efficiencies in the mixed electrolytes approaches η in pure NaCl electrolyte (Figure 6c). The current efficiencies with θ = 0.33 are equal to the ones in pure NaCl electrolyte except for the current density of 40 A cm^{-2}. At this current density, the current efficiency is η = 97 % in mixed electrolyte with θ = 0.33. This value is in between the values obtained in the pure chloride and nitrate electrolytes.

Also the surface quality obtained in the mixed electrolyte (Figure 9e and g) appears similar to those obtained in pure NaCl electrolyte (Figure 9d and f) at 10 A cm^{-2} and 20 A cm^{-2}. The S_a values indicate that the chloride dissolution mechanism dominates. Lower current densities show a slightly different behaviour. Figure 9b shows the surface obtained at 5 A cm^{-2} in mixed electrolyte with θ = 0.33 and γ = 0.167. It is rougher than those obtained in pure NaCl with the same γ (Figure 9a) and in mixed electrolyte with the same mixing ratio and larger duty cycle of γ = 0.5 (Figure 8b). A value S_a > 1 µm indicates that under these specific conditions a higher roughness is obtained in the presence of both anions. Perhaps the chloride ion flux towards the surface is insufficient with respect to competing nitrate anions. At higher current densities of 40 A cm^{-2} in a mixed electrolyte with θ = 0.33 (Figure 9i) the surface show features found on surfaces obtained

in both pure NaCl and $NaNO_3$ electrolytes (Figures 9h and 9j). It is concluded that both mechanisms proceed simultaneously at the same regions of a surface (in contrast to the situation found in Figure 7d). Applying different duty cycles in series was tested with γ = 0.625 (Q = 200 C), 0.5 (50 C) and 0.167 (50 C) at 5 A cm^{-2} with θ = 0.33 in order to assess the surface quality after each step.

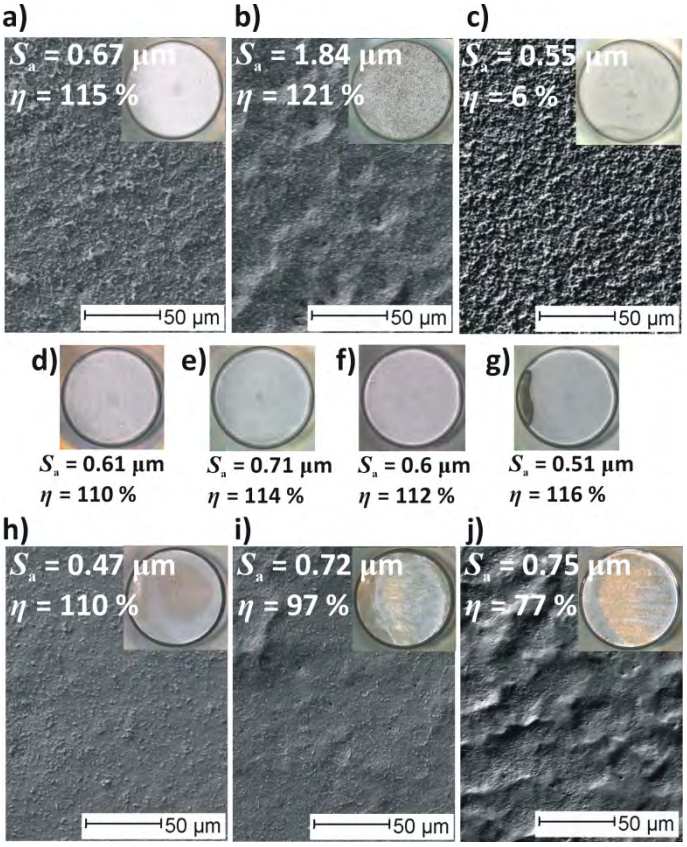

Figure 9. *Comparison of resulting surfaces with γ = 0.167. Electrolyte flow direction in optical micrographs and in SEM micrographs is from left to right.* ***(a)*** *j = 5 A cm^{-2}, θ = 1.* ***(b)*** *j = 5 A cm^{-2}, θ = 0.33.* ***(c)*** *j = 5 A cm^{-2}, θ = 0.* ***(d)*** *j = 10 A cm^{-2}, θ = 1.* ***(e)*** *j = 10 A cm^{-2}, θ = 0.33.* ***(f)*** *j = 20 A cm^{-2}, θ = 1.* ***(g)*** *j = 20 A cm^{-2}, θ = 0.33.* ***(g)*** *j = 40 A cm^{-2}, θ = 1.* ***(i)*** *j = 40 A cm^{-2}, θ = 0.33.* ***(j)*** *j = 40 A cm^{-2},θ = 0.*

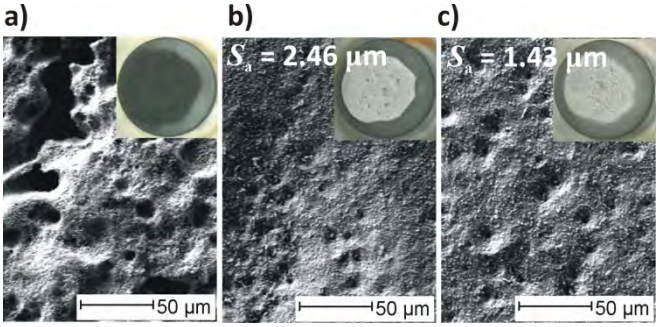

Figure 10. *Comparison of resulting surfaces after anodic dissolution in series with variation of duty cycle*; j = *5 A cm^{-2},* θ = 0.33. ***(a)*** *γ = 0.625; Q = 200 C;* ***(b)*** *i. γ = 0.625; Q = 200 C, ii. γ = 0.5; Q = 50 C;* ***(c)*** *i. γ = 0.625; Q = 200 C, ii. γ = 0.5; Q = 50 C, iii. γ = 0.167; Q = 50 C. Electrolyte flow direction in optical micrographs and in SEM micrographs is from left to right.*

In Figure 10, three specimens are shown, one processed just with the first step (Figure 10a), the second processed with the first two steps (Figure 10b) and the third processed with all three steps

(Figure 10c). The conditions in Figure 10a were identical to Figure 7d except for the use of a lower charge (200 C instead of 300 C). Because both dissolution mechanisms take place simultaneously, a black porous surface is observed (Figure 10a). However, less material is removed in Figure 10a than in Figure 7b causing a less distinctive porosity. S_a is still larger than the measurable range. The next step (γ = 0.5) in which the dissolution is dominated by chloride anions efficiently removes the black surface (Figure 10b). Only a few pits and an edge at transition from flat plateau to the rim of specimen remain. Applying all three steps decreases the roughness in the last step (Figure 10c). The last step in which chloride anions dominate the dissolution flattens the surface and a smooth transition to the rim of the specimen is achieved. A look at the SEM micrograph shows that the surface is equal to the one in Figure 9b with the same duty cycle and chloride anion ratio (γ = 0.167, θ = 0.33).

Conclusions

The anodic dissolution of 100Cr6 in chloride/nitrate mixed electrolytes was investigated. LSV at RDE assuming mainly laminar flow conditions showed that either active or transpassive dissolution can be achieved by controllable mass transport conditions (bulk chloride concentration and rotation rate). This is indicated by an abrupt decrease in current density with increasing anodic potential. While active dissolution due to chloride-dominated mechanism takes place at lower current densities, transpassive dissolution due to nitrate-anion dominated mechanism is observed at higher current densities. By changing the potential or current density, it is possible to switch reversibly between both dissolution mechanisms.

The following dissolution mechanism is proposed. If the flux of chloride ions relative to the current density is too small, the chloride anion mechanism cannot be maintained and transpassive dissolution due to nitrate-dominated dissolution commences. This transpassive dissolution is then stable in the observed current density ranges. The anodic dissolution is mass transport-controlled and depends on the anode/electrolyte interface layer.

Flow channel experiments applying galvanostatic pulses showed that under assumed turbulent flow conditions a separation of dominating dissolution mechanisms can be observed under specific conditions while both mechanisms may also proceed simultaneously under other conditions. There is not only an influence of anion ratio but also on current density, pulse parameters and flow conditions.

Acknowledgements: *The technical assistance by Ms. Carmen Pritsch is acknowledged.*

References

[1] A. D. Davydov, V. M. Volgin in *Encyclopedia of Electrochemistry* (D.D. Macdonalds, P. Schmuki Eds.) Wiley, Vol. **5,** 2007pp. 809-854.
[2] J. A. McGeough, M. B. Barker, *Chemtech* **21** (1991) 536-542.
[3] M. Datta, D. Landolt, *Electrochim. Acta* **26** (1981) 899-907.
[4] D. T. Chin, K. W. Mao, *J. Appl. Electrochem.* **4** (1974, 155-161.
[5] M. Datta, D. Landolt, *Electrochim. Acta* **25** (1980) 1255-1262.
[6] M. Datta, D. Landolt, *Electrochim. Acta* **25** (1980) 1263-1271.
[7] T. Haisch, E. Mittemeijer, J. W. Schultze, *Electrochim. Acta* **47** (2001) 235-241.
[8] M. M. Lohrengel, *Mater. Manuf. Process.* **20** (2005) 1-8.
[9] K.-W. Mao, M. A. LaBoda, J. P. Hoare, *J. Electrochem. Soc.* **119** (1972) 419-427.
[10] K.-W. Mao, *J. Electrochem. Soc.* **118** (1971) 1876-1879.
[11] M. M. Lohrengel, C. Rosenkranz, D. Rohrbeck, *Microchim. Acta* **156** (2006) 163-166.

[12] C. Rosenkranz, M. M. Lohrengel, J. W. Schultze, *Electrochim. Acta* **50** (2005) 2009-2016.
[13] T. Haisch, E. J. Mittemeijer, *Jom* **54** (2002) 38-41.
[14] T. Haisch, E. J. Mittemeijer, J. W. Schultze, *Mater. Corros.* **53** (2002) 740-755.
[15] T. Haisch, E. J. Mittemeijer, J. W. Schultze, *J. Appl. Electrochem.* **34** (2004) 997-1005.
[16] M. M. Lohrengel, I. Kluppel, C. Rosenkranz, H. Bettermann, J. W. Schultze, *Electrochim. Acta* **48** (2003) 3203-3211.
[17] J. P. Hoare, M. A. LaBoda, *Comprehensive Treatise of Electrochemistry,* Plenum Press, New York, 1981, pp. 806.
[18] K.-W. Mao, J. P. Hoare, *Corr. Sci.* **13** (1973) 799-803.
[19] H. McCrabb, A. Lozano-Morales, S. Snyder, L. Gebhart, E. J. Taylor, *T.Electrochem. Soc.* **19** (2009) 19-33.
[20] S. Moser, Thesis, Heinrich-Heine-University of Düsseldorf (2004).
[21] M. Datta, *IBM J. Res. Dev.* **37** (1993) 207-226.
[22] H. C. Kuo, D. Landolt, *Electrochim. Acta* **20** (1975) 393-399.
[23] A. D. Davydov, A. N. Kamkin, *Elektrokhimiya* **14** (1978) 979-992.
[24] V. G. Levich, *Physicochemical Hydrodynamics*, Prentice Hall, 1962.
[25] D. R. Lide, *CRC handbook of chemistry and physics*, CRC Press, Boca Raton, Fla., 2006.
[26] A. J. Bard, L. R. Faulkner, *Electrochemical Methods: Fundamentals and Applications*, John Wiley & Sons, New York, 2001, p. 347.